Transactions of the 15th International Conference on
Structural Mechanics in Reactor Technology (SMiRT-15)
Seoul, Korea, August 15-20, 1999

Geometrically Nonlinear Analysis of Thin-Walled Space Frames

Sung Pil Chang[1], Hyo Gi Park[1], Moon Young Kim[2] and Sung Bo Kim[3]

1) Seoul National University, Korea
2) Sung Kyun Kwan University, Korea
3) Chungbuk National University, Korea

ABSTRACT

A clearly consistent finite element formulation for geometrically non-linear analysis of thin-walled space frames is presented by applying incremental equilibrium equations based on the updated Lagrangian formulation and introducing Vlasov's assumption. The improved displacement field for non-symmetric thin-walled cross sections is introduced based on inclusion of second order terms of finite rotations, and the potential energy corresponding to the semitangential rotations and moments is consistently derived. For finite element analysis, elastic and geometric stiffness matrices of thin-walled space frame element with 7 degrees of freedom per each node are derived. In iterative non-linear analysis, local coordinates are updated and the incremental member forces are evaluated by separating the rigid body rotations and pure deformations from incremental displacements.

1. INTRODUCTION

The large deformation and stability analyses of thin-walled structures have been the major research field in structural division of civil, mechanical and aerospace engineering. However, it is well known that the thin-walled members display complex structural behaviors and particularly, are very susceptible to spatial post-buckling behaviors. Recently, according to the development of the high speed digital computer, the numerical technique of the post-buckling analysis has advanced remarkably.

For the geometrically non-linear analysis of space frame, Wen and Rahimzadeh[1], Bathe and Bolourchi[2] used the straight and curved element, respectively. Saafan[3] investigated the non-linear behavior of structural plane frames considering the change of horizontal displacement due to the bending deformation. Meek and Tan[4] and Papadrakakis[5] presented the post-buckling analysis of space frame using the arc-length method and the vector iteration method, respectively. Kim and Chang[6] formulated the geometrically non-linear analysis for plane and space frame element using load and displacement incremental algorithm.

On the other hand, considering spatial stability and geometric non-linear analysis of space frames which consist of structural members with different directions in space, Argyris et al.[7] pointed out that most of previous finite element formulations which include only the first order terms of rotational parameters of the cross section appear to be incorrect. It is largely due to deficiency of moment equilibrium conditions at the joint and the non-commutative nature of rotations about fixed axes. In order to circumvent these difficulties, Argyris et al.[8] introduced the semitangential moment and the semitangential rotation that have mechanical corresponding to Ziegler's[9] semitangential torque, and derived the geometric stiffness matrix of the space frame with bisymmetric cross-section using the natural mode formulation and ignoring warping effects. Kuo et. al[10] presented non-linear analysis of space frames considered finite rotations.

In this paper, a clearly consistent finite element formulation for geometrically non-linear analysis of thin-walled space frames is presented based on the co-rotational formulation by applying the principle of virtual work and introducing Vlasov's assumption. According to the displacement field based on inclusion of second order terms of finite rotations, the potential energy corresponding to the semitangential rotations and moments is consistently derived. Tangent stiffness matrices including warping deformations are derived using the Hermitian polynomials as shape functions. By separating the rigid body rotations and pure deformations from incremental displacements, and calculating the incremental member forces from pure deformations, the unbalanced loads are precisely evaluated. Numerical solutions for the post-buckling analysis of thin-walled space frames are presented in order to illustrate the accuracy and practical usefulness of this formulation.

2. GEOMETRICALLY NON-LINEAR FINITE ELEMENT FORMULATION

2.1 Displacement Parameters and Stress Resultants

Displacement measures for a thin-walled cross-section with right-handed coordinate system observed from the positive x_1 axis are shown in Fig. 1.(a) The x_1 axis is the member axis defined at the centroid. x_2 , x_3 are the principal inertia axes; U_x , U_y , U_z are rigid body translations of the cross-section in the x_1, x_2 and x_3 direction, respectively; θ, $-U_z'$, U_y' are rigid body rotations about the x_1, x_2 and x_3 axes, respectively; θ' is a parameter defining warping of the cross-section.

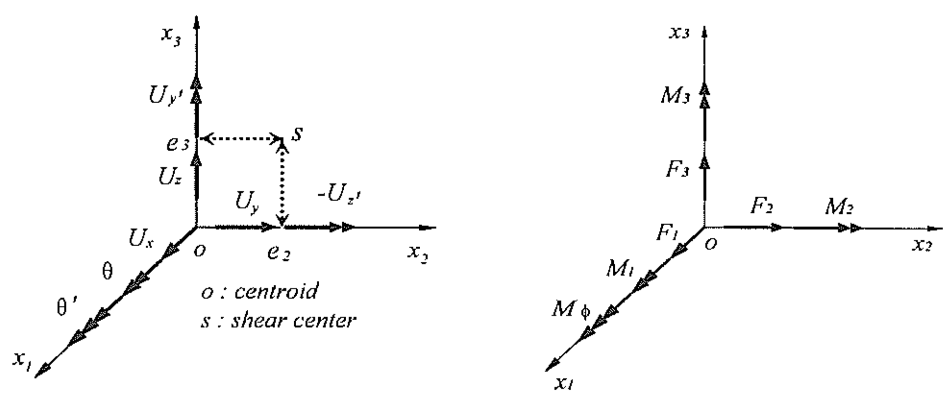

(a) Displacement parameters (b) Stress resultants

Fig. 1. Notation for displacement parameters and stress resultants

Two cartesian coordinate system are defined in order to introduce displacement parameters, section properties and stress resultants. The axes of (x_2, x_3) at centroid and (x_2^s, x_3^s) at shear center are parallel to principal axes, respectively, and e_2 , e_3 are coordinates of the shear center. The relationship of two axes is as follows,

$$\begin{aligned} x_2 &= x_2^s + e_2 \\ x_3 &= x_3^s + e_3 \end{aligned} \tag{1}$$

The incremental displacement is expressed by the sum of U_i and U_i^* which are due to the first and second order terms of the displacement parameters, respectively, and their detailed terms are as following,

$$U_1(x_1, x_2, x_3) = U_x - U_z' x_3 - U_y' x_2 - \theta' \phi \tag{2a}$$
$$U_2(x_1, x_2, x_3) = U_y - \theta x_3 \tag{2b}$$
$$U_3(x_1, x_2, x_3) = U_z + \theta x_2 \tag{2c}$$

and

$$U_1^*(x_1, x_2, x_3) = \frac{1}{2}[-\theta U_z' x_2 + \theta U_y' x_3] \tag{3a}$$
$$U_2^*(x_1, x_2, x_3) = \frac{1}{2}[-(\theta^2 + U_y'^2) x_2 - U_y' U_z' x_3] \tag{3b}$$
$$U_3^*(x_1, x_2, x_3) = \frac{1}{2}[-(\theta^2 + U_z'^2) x_3 - U_y' U_z' x_2] \tag{3c}$$

In (2a), ϕ is the warping function defined at the centroid and ϕ^s at the shear center. Relations of two warping functions is expressed as

$$\phi = \phi^s - x_2 e_3 + x_3 e_2 \tag{4}$$

On the other hand, section properties are defined as follows,

$$\begin{aligned} I_2 &= \int_A x_3^2 \, dA \quad , \quad I_3 = \int_A x_2^2 \, dA \\ I_{2\phi} &= \int_A x_3 \phi \, dA \quad , \quad I_{3\phi} = \int_A x_2 \phi \, dA \\ I_\phi &= \int_A \phi^2 \, dA \end{aligned} \tag{5}$$

The warping functions defined at Eq. (4) are satisfied by following equations.

$$S_\phi = \int_A \phi \, dA = 0 \quad , \quad S_\phi^s = \int_A \phi^s \, dA = 0 \tag{6}$$

Considering Eq. (4), (5) and (6), the relation of section properties defined at two coordinate systems is as follows,

$$\begin{aligned} I_{3\phi} &= -I_3 e_3 \quad , \quad I_{2\phi} = I_2 e_2 \\ I_\phi &= I_\phi^s + I_3 e_3^2 + I_2 e_2^2 \end{aligned} \tag{7}$$

Actually assuming plane stress state ($\tau_{22} = \tau_{33} = \tau_{23} = 0$), stress resultants can be defined as

$$F_1 = \int_A \tau_{11}\, dA \quad , \quad F_2 = \int_A \tau_{12}\, dA \quad , \quad F_3 = \int_A \tau_{13}\, dA$$
$$M_1 = \int_A (\tau_{13} x_2 - \tau_{12} x_3)\, dA$$
$$M_2 = \int_A \tau_{11} x_3\, dA \quad , \quad M_3 = -\int_A \tau_{11} x_2\, dA$$
$$M_\phi = \int_A \tau_{11} \phi\, dA \quad , \quad M_R = \int_A (\tau_{12} \phi_{,2} + \tau_{13} \phi_{,3})\, dA$$
$$M_P = \int_A \tau_{11}[\ (x_2 + x_3)^2\ ]\, dA \tag{8}$$

In above equations, F_1, F_2 and F_3 are the axial force, the shear forces, respectively; M_2 and M_3 are bending moments with respect to x_2 and x_3 axes, respectively; M_1 is the total twist moment; M_R and M_ϕ are the restrained(non-uniform) torsional moment and the bimoment, respectively. M_P is a stress resultant defined as Eq. (8) and is known as the Wagner effect[Chen and Atuta[11]].

Assuming the linear elastic material and substituting the linear strain displacement relations into Eq.(8), the force-displacement relations are obtained as

$$F_1 = EA\, U_x' \ , \quad F_2 = M_3' \ , \quad F_3 = -M_2' \ , \quad M_1 = GJ\theta'$$
$$M_2 = -EI_2\, U_z'' - EI_{3\phi}\, \theta'' \ , \quad M_3 = EI_3\, U_y'' + EI_{2\phi}\, \theta''$$
$$M_\phi = -EI_{3\phi}\, U_z'' - EI_{2\phi}\, U_y'' - EI_\phi\, \theta'' \tag{9}$$

2.2 Incremental Equilibrium Equation and Tangent Stiffness Matrix

The incremental equilibrium equation is expressed as follows,

$$\int_{^tV} {}_tC_{ijrs}\, {}_te_{rs}\, \delta\, {}_te_{ij}\, d^tV + \int_{^tV} {}^t\tau_{ij}\, \delta(\, {}_t\eta_{ij} + {}_te_{ij}^*)\, d^tV = {}^{t+\Delta t}R - \int_{^tV} {}^t\tau_{ij}\, \delta\, {}_te_{ij}\, d^tV \tag{10}$$

where,
$$ {}_te_{ij} = \frac{1}{2}(\, {}_tU_{i,j} + {}_tU_{j,i}) \quad , \quad {}_t\eta_{ij} = \frac{1}{2}(\, {}_tU_{k,i} \cdot {}_tU_{k,j})$$
$$ {}_te_{ij}^* = \frac{1}{2}(\, {}_tU_{i,j}^* + {}_tU_{j,i}^*) \tag{11}$$

No superscript represents the incremental variable. ${}^t\tau_{ij}$ is the Cauchy stress at time t; U_i and U_i^* denote incremental displacements due to the first and second order effects of the rotational displacement parameters, respectively.

Substituting the displacements expansion Eq. (2) and Eq. (3) into Eq. (10) and noting the definition equation of stress resultants, Eq. (10) is reduced to the following equations.

$$\int {}_tC_{ijrs}\, {}_te_{rs}\, \delta\, {}_te_{ij}\, d^tV$$
$$= \frac{1}{2}\,\delta \int (\, EA\, U_x'^2 + EI_3 U_y''^2 + EI_2 U_z''^2 + GJ\theta'^2 + EI_\phi \theta''^2)\, {}^tdx_1 \tag{12a}$$

$$\int {}^t\tau_{ij}\, \delta (\, {}_t\eta_{ij} + {}_te^*_{ij})\, d^tV$$
$$= \frac{1}{2}\,\delta \int [\, {}^tF_1 (U_y'^2 + U_z'^2) + {}^tM_P\, \theta'^2 + {}^tF_2\, U_z'\, \theta - {}^tF_3\, U_y'\, \theta \tag{12b}$$
$$+ {}^tM_1 (U_z'\, U_y'' - U_z''\, U_y') + {}^tM_2 (U_y''\, \theta - U_y'\, \theta') + {}^tM_3 (U_z''\theta - U_z'\theta')\,]\, {}^tdx_1$$

$$\int {}^t\tau_{ij}\, \delta\, {}_te_{ij}\, d^tV$$
$$= \int [\, {}^tF_1\, \delta U_x' - {}^tM_2\, \delta U_z'' + {}^tM_3\, \delta U_y'' + {}^tM_1\, \delta\theta' - {}^tM_\phi\, \delta\theta''\,]\, {}^tdx_1 \tag{12c}$$

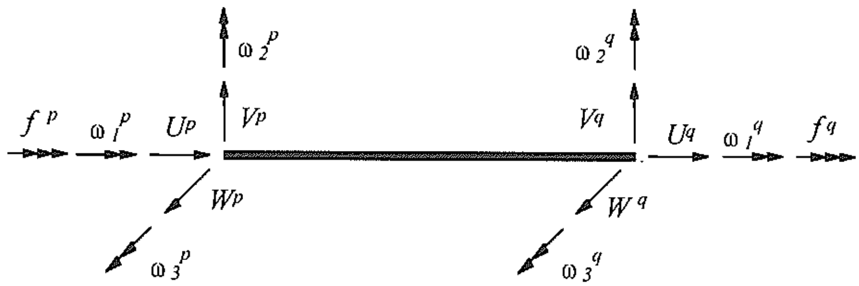

Fig. 2. Member displacement vector

Fig. 2. shows the member displacement vector of a thin-walled space frame element. In this study, the axial displacement U_x is assumed to be linear function, and the lateral displacements U_y , U_z and twist angle θ is interpolated by cubic Hermitian shape functions as

$$U_x = (1 - \xi) \cdot U^p + \xi \cdot U^q \ , \quad \xi = x_1 / L \tag{13a}$$
$$U_y = h_1 \cdot V^p + h_2 \cdot L \cdot \omega_3^p + h_3 \cdot V^q + h_4 \cdot L \cdot \omega_3^q \tag{13b}$$
$$U_z = h_1 \cdot W^p - h_2 \cdot L \cdot \omega_2^p + h_3 \cdot W^q - h_4 \cdot L \cdot \omega_2^q \tag{13c}$$
$$\theta = h_1 \cdot \omega_1^p - h_2 \cdot L \cdot f^p + h_3 \cdot \omega_1^q - h_4 \cdot L \cdot f^q \tag{13d}$$

Substituting Eq. (13) into Eq. (12) and integrating along the element length, the incremental equilibrium Eq. (10) is reduced to

$$\delta U_e^{\,T}\, {}^tK_e\, U_e = {}^{t+\Delta t}R - \delta U_e^{\,T}\, {}^tF_e \tag{14a}$$

where,

$$U_e = \langle\, U^p, V^p, W^p, \omega_1^p, \omega_2^p, \omega_3^p, f^p, U^q, V^q, W^q, \omega_1^q, \omega_2^q, \omega_3^q, f^q \rangle \tag{14b}$$
$${}^tF_e = \langle\, {}^tF_1^p, {}^tF_2^p, {}^tF_3^p, {}^tM_1^p, {}^tM_2^p, {}^tM_3^p, M_\phi^p, {}^tF_1^q, {}^tF_2^q, {}^tF_3^q, {}^tM_1^q, {}^tM_2^q, {}^tM_3^q, {}^tM_\phi^q \rangle \tag{14c}$$

U_e and $'F_e$ are the incremental displacement and member force vector, respectively, shown in Fig. 2. '< >' denotes the row vector.

2.3 Calculation of the Unbalanced Force

In the non-linear analysis of a structure, an iterative calculation is adopted and it is very important that the member force is precisely calculated at the deformed state. In iterative evaluation based on the updated Lagrangian co-rotational formulation, the incremental member displacement U_e is separated by rigid body displacement U_r and pure deformation U_d as following

$$U_t = \langle\, U_r \;\vdots\; U_d \,\rangle \tag{15a}$$

where,

$$U_r = \langle\, u_r, v_r, w_r, \gamma_1, \gamma_2, \gamma_3 \,\rangle \tag{15b}$$

$$U_d = \langle\, u, \theta_{13}, \theta_{23}, \theta_{12}, \theta_{22}, \omega, f^p, f^q \,\rangle \tag{15c}$$

In Eq. (15b) and Eq. (15c), $\langle u_r, v_r, w_r \rangle$ and $\langle \gamma_1, \gamma_2, \gamma_3 \rangle$ are the rigid body translation and rotation, respectively, and can be evaluated by the following equation.

$$u_r = (U^p + U^q)/2 \;;\quad v_r = (V^p + V^q)/2 \;;\quad w_r = (W^p + W^q)/2 \tag{16a-c}$$

$$\gamma_1 = (\omega_1^q + \omega_1^p)/2 \;;\quad \gamma_2 = (-W^q + W^p)/L \;;\quad \gamma_3 = (V^q - V^p)/L \tag{16d-f}$$

$$u = U^q - U^p \;;\quad \omega = \omega_1^q - \omega_1^p \;;\quad f^p = f^p \;;\quad f^q = f^q \tag{16g-j}$$

$$\theta_{12} = \omega_2^p - \gamma_2 \;;\quad \theta_{22} = \omega_2^q - \gamma_2 \;;\quad \theta_{13} = \omega_3^p - \gamma_3 \;;\quad \theta_{23} = \omega_3^q - \gamma_3 \tag{16k-n}$$

where θ_{13}, θ_{23}, θ_{12}, θ_{22} are the incremental member end rotation as shown in Fig. 3; u and ω are the relative incremental axial displacement and twist angle, respectively; f^p and f^q are the incremental warping parameter of the member end, respectively.

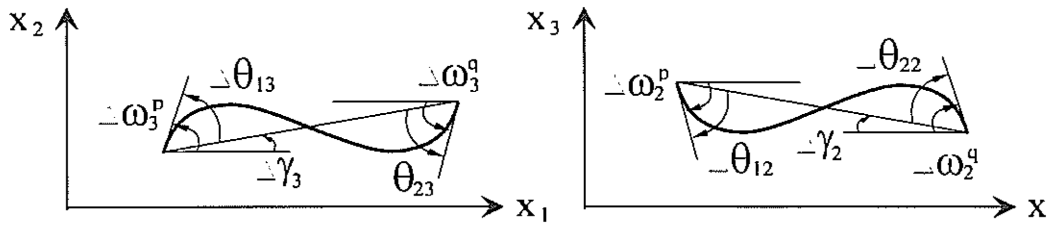

Fig. 3. Pure deformations of the beam in the x_1-x_2 and x_1-x_3 plane

Considering Eq. (15) and Eq. (16), the relation between U_e and U_t is constructed by the compatibility matrix A_e as follows,

$$U_e = A_e \cdot U_t \tag{17}$$

Substituting Eq. (17) into Eq. (14a), the tangent stiffness matrix ${}^tK_t$ corresponding to the incremental displacement U_t is obtained as,

$$\delta U_e{}^T \, {}^tK_e \, U_e = \delta U_t{}^T (A_e{}^T \, {}^tK_e \, A_e) \, U_t = \delta U_t{}^T \, {}^tK_t \, U_t \tag{18}$$

The 8×8 matrix, ${}^tK_{td}$ means the tangent stiffness corresponding to the pure deformation U_d. Resultantly, the incremental member force F_d is evaluated by

$$K_{td} \cdot U_d = F_d \tag{19a}$$

where, $$F_d = \langle F \, , M_{13} \, , M_{23} \, , M_{12} \, , M_{22} \, , M_1 \, , M_\phi^p \, , M_\phi^q \rangle \tag{19b}$$

In geometrically non-linear analysis of space frame, Bowing effect, i.e. the relative axial displacement due to the flexural and torsional deformation, need be considered. Therefore, when calculating the member force, (16g) for the axial deformation u should be modified as

$$u = U^q - U^p + \Delta \tag{20a}$$

$$\Delta = (\theta_{12}{}^2 + \theta_{22}{}^2 + \theta_{13}{}^2 + \theta_{23}{}^2) \frac{L}{15} - (\theta_{12}\,\theta_{22} + \theta_{13}\,\theta_{23}) \frac{L}{30} + \frac{(I_2 + I_3) \, \omega^2}{2A} \tag{20b}$$

Applying the coordinate transformation and direct stiffness method, the incremental equilibrium equation for the entire structure is obtained. After that the incremental displacement in global coordinate is calculated, the incremental member force and the unbalanced force are obtained. Also, the unbalanced force are used as the applied force in the next iteration step.

3. NUMERICAL EXAMPLES

3.1 Lateral Buckling of Right Angle Frame under End Moment

Fig. 4. show a cantilever right-angle frame subjected to a semitangential moment. The sectional parameters are listed below.

$L = 100 cm$ $\quad A = 1 \, cm^2$ $\quad I_y = 1000 \, cm^4$ $\quad I_z = 1 \, cm^4$

$E = 10^4 N/cm^2$ $\quad G = E/2$ $\quad J = 2 cm^4$

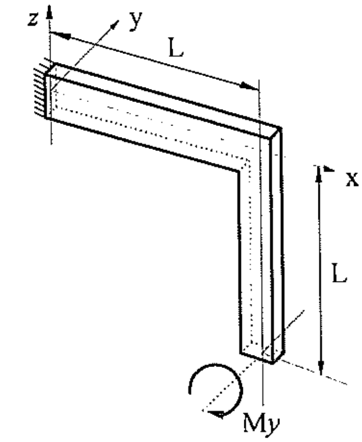

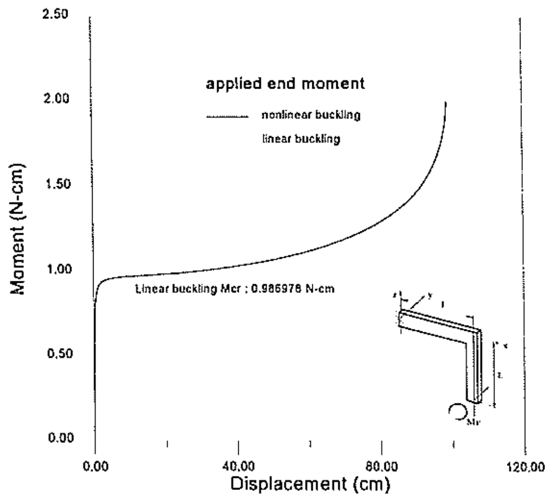

Fig. 4. Lateral buckling of right-angle frame   Fig. 5. Load-displacement diagram

The buckling behavior of the right angle frame under a semitangential moment M_y is investigated. The critical buckling moment by this study are identical to the result by Argyris[1]. The semitangnetial moment is applied according to the generating method defined by Argyris[1] and also, the lateral imperfection load $P_y (= \frac{M_y}{1000})$ is loaded in the y-direction. During pre- and post-buckling, the plot of the load parameter versus lateral displacement at the free end is presented in Fig. 5. The lateral-torsional post-buckling behavior is observed after the end moment reaches the linear buckling moment.

3.2 Cantilever Right-Angle Frame with I-Type Cross-Section under Lateral Load

Fig. 6. show a cantilever right-angle frame under end load and its I-type cross-section corresponding to W21×93. In this case, the joint condition connecting horizontal member and vertical member can be classified as warping-free, warping-partially restrained and warping-fully restrained connections according to types of connections. In this study, three methods are used in order to investigate the lateral buckling of the cantilever frame with warping-free and warping-fully restrained connections.

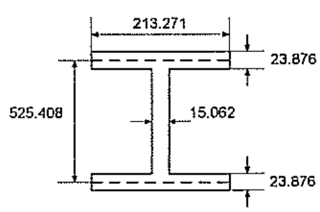

$L = 6096\,mm$	$A = 17612.868\,mm^2$
$I_y = 8.616\times10^8\,mm^4$	$I_z = 3.867\times10^7\,mm^4$
$J = 2.510\times10^6\,mm^4$	$I_\phi = 2.669\times10^{12}\,mm^{12}$
$E = 199948\,MPa$	$G = 76904.2\,MPa$

(a) I-type cross section(W21x93)

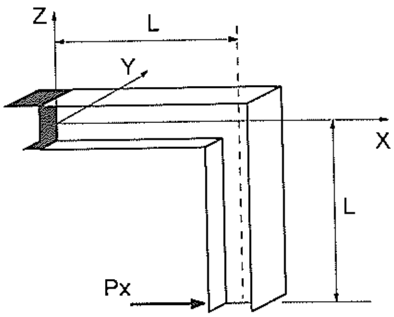

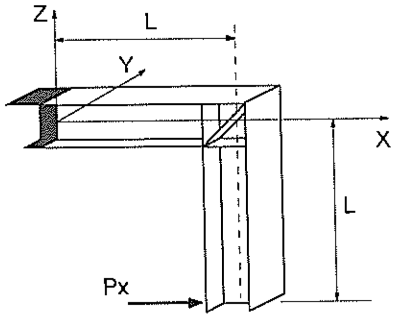

(b) Two connection types of cantilever frame with I-type cross section
Fig. 6. Cantilever right-angle frames with I-type section under end load

Table 1. Critical load of I-type right-angle frames under end load(kN)

Method 1 (1)		Method 2 (2)		Method 3 (3)	
-52.367	59.042 56.619*	-59.660	65.414 66.234**	-69.129	80.604 81.366**
** : Saleeb et al.[12] * : Yang and McGuire[13]					

Using these methods, the lateral buckling loads of the cantilever frame are presented in Table 1 with results by Saleeb et al.[12] and Yang and McGuire[13]. Method 1 denotes the scheme of the finite element buckling analysis in which all element stiffness matrices are assembled directly, so the bimoments of the connection between the horizontal and vertical member are added. Method 2 denotes the scheme in which the bimoment of either the horizontal or the vertical member is assembled in constructing the global tangent stiffness matrix. Method 3 means the same as method 2 except for fully fixed constraint of the warping degree of freedom at the connection joint.

Fig. 7. shows load-displacement diagram of this right-angle frames under positive and negative load, respectively. In order to trace well the non-linear behavior, the lateral imperfection load in y-axis($P_y = P_x/1000$) is applied. It can be seen that the large displacement of the free end is occurred when the end load reached the linear buckling load.

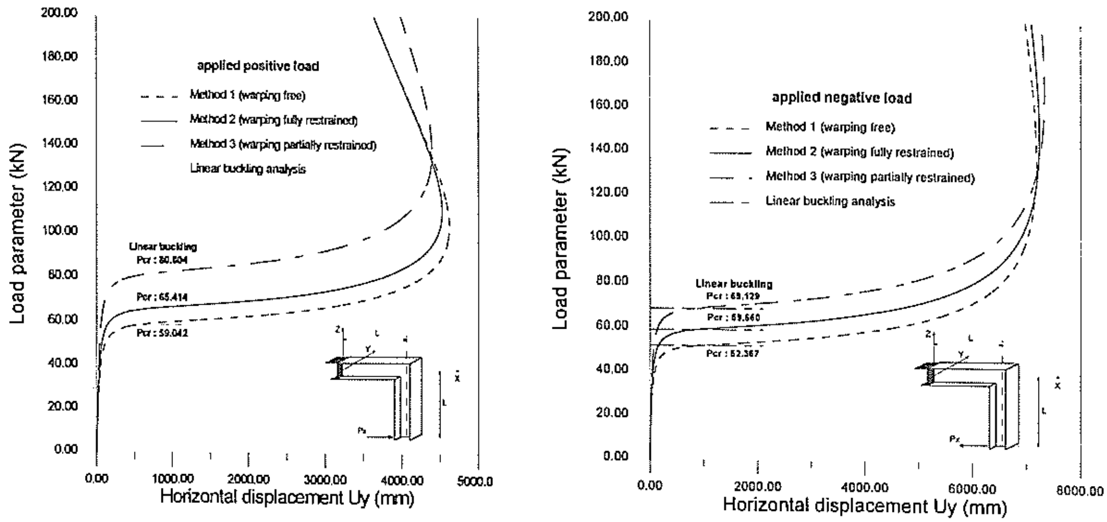

(a) positive end load (b) negative end load

Fig. 7. Load-displacement diagram for end load

3.3 Straight and Curved Cantilever Beam with Monosymmetric Cross-Section under Lateral Load

The total number of finite elements is twenty. Fig. 8.(a) shows the sectional and material properties of monosymmetric section. Fig. 8.(b) and Fig. 8.(c) show the straight and curved cantilever beam subjected to axial load at the tip.

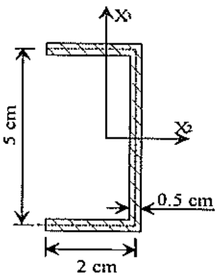

$A = 8.0\ cm^2$ $E = 30,000\ N/cm^2$ $G = 11,500\ N/cm^2$

$J = 0.375\ cm^4$ $e_2 = 1.15032\ cm$ $I_2 = 17.7500\ cm^4$

$I_3 = 1.8299\ cm^4$ $I_\phi = 31.3309\ cm^4$ $I_{\phi 2} = -20.4183\ cm^6$

$\beta_1 = 4.35108\ cm^2$ $\beta_3 = -0.33038$

(a) Monosymmetric cross-section and section properties

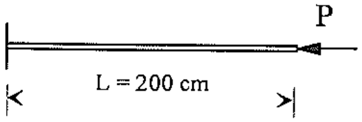

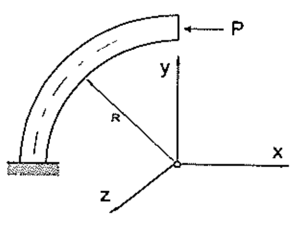

(b) Straight cantilever beam under axial load (c) Curved cantilever beam under axial load

Fig. 8. Straight and curved cantilever beam with monosymmetric cross-section

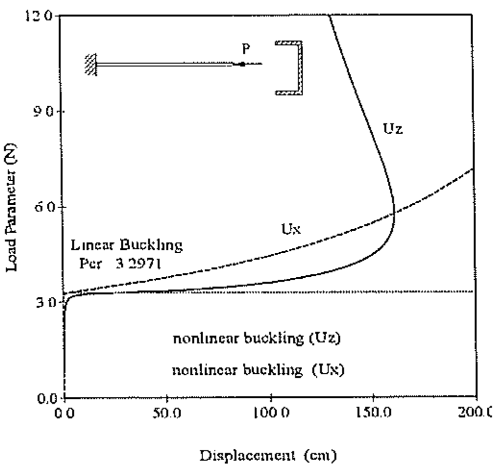

Fig. 9. Load-displacement diagram of straight cantilever beam

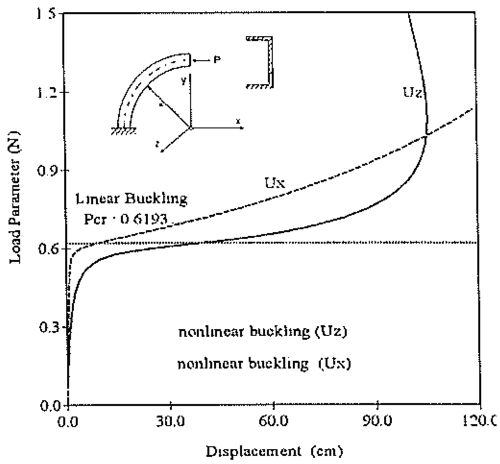

Fig. 10. Load-displacement diagram of curved cantilever beam

Fig. 9 and Fig. 10 show the non-linear behaviors of the straight and curved cantilever beam subjected to axial end load in x-direction, respectively. In order to trace well the post-buckling behavior, the lateral imperfection load in z-axis($P_z = P_y/1000$) is applied. In these figures, it is shown that the predicted buckling load resulting in the large displacement of the free end is almost same as the linear bifurcation load and typical post-buckling behaviors are traced at load levels higher than the linear buckling load. .

4. CONCLUSIONS

By introducing Vlasov's assumption and degenerating incremental eqautions for 3D continuum to those for thin-walled space frames, a clearly consistent F. E. formulation is presented based on the co-rotational formulation. The improved displacement field for non-symmetric thin-walled cross sections is introduced based on inclusion of second order terms of finite semitangential rotations. A scheme for calculation of the unbalanced load vector consistently is presented by separating rigid body rotations and pure deformations from incremental displacements, and evaluating the transformed tangent stiffness matrix corresponding to pure deformations. In order to illustrate the accuracy and practical usefulness of these formulations, finite element solutions for the spatial buckling and post-buckling analysis of thin-walled space frames are compared with available solutions. As a result, the following conclusions are drawn:

1. In case of the linear bifurcation buckling load of space frames neglecting restrained warping effects, the results by this study are identical to those of Argyris. It is resulted from that the present stiffness matrix considering the second order terms of finite semitangential rotations, is almost the same as those of Argyris using the natural mode formulation.
2. This finite element formulation is applicable to geometrically non-linear analysis of the thin-walled space frames with non-symmetric cross sections subjected to the semitangential moment as well as the lateral load.

3. The straight thin-walled space frame element developed in this study is applicable for lateral-torsional buckling and post-buckling analysis of not only space frames but also thin-walled curved beams with any configuration.

ACKNOWLEDGEMENTS

The financial support of POSCO research fund to the authors is gratefully acknowledged. The authors are grateful for the support provided by a grant from the Korea Science & Engineering Foundation(KOSEF) and Safety and Structural Integrity Research Center at the Sungkyunkwan University.

REFERENCES

1. Wen, R. K. and Rahimzadeh, J., "Nonlinear elastic frame analysis by finite element. " *J. Struct. Engrg., ASCE*, 109, 1952-1971.,1983
2. Bathe, K. J. and Bolourchi, S., "Large displacement analysis three-dimensional beam structures." *Int. J. Numer. Methods Engrg.*, 14, 961-986.,1979
3. Saafan, S. A., "Non-linear behavior of structural plane frames." J. *Struct. Engrg., ASCE,* 89, 557-579., 1963
4. Meek, J. L. and Tan, H. S., "Geometrically nonlinear analysis of space frames by an incremental iterative technique." *Comp. Methods in Appl. Mech. and Engrg.*, 14, 261-282.,1984
5. Papadrakakis, M., "Post-buckling analysis of spatial structures by vector iteration methods. ", *Comp. and Struct.*, 14, 393-402.,1990
6. Kim, M. Y., Chang, S. P., "Geometrically non-linear analysis of the plane frame structures including shear deformation effects." *J. of Korea society of civil engrg.*, 10(1), 27-36.,1990
7. Argyris, J. H., Dunne, P. C. and Scharpf, D. W.,"On large displacement-small strain analysis of structures with rotational degrees of freedom." *Comp. Methods in Appl. Mech. and Engrg.*, 14, 401-451.,1978
8. Argyris, J. H., Hilpert, O., Malejannakis, G. A. and Scharpf, D. W., "On the geometrical stiffness of a beam in space - a consistent v. w. approach." *Comp. Methods in Appl. Mech. and Engrg.*, 20, 105-131.,1979
9. Ziegler, H., *Principles of structural stability*, 2nd ed., Birkhaser, Basel/Stuttgart. ,1977
10. Kuo, S. R., Yang, Y. B., and Chou, J. H., "Nonlinear analysis of space frames with finite rotations.", *J. Struct. Engrg., ASCE,* 119(1), 1-15.,1993
11. Chen, W. F. and Atsuta, T., *Theory of beam-columns, Vol. 2, Space behavior and design*, McGraw-Hill, New York., 1977
12. Saleeb, A. F., Chang, T. Y. P. and Gendy, A. S., "Effective modelling of spatial buckling of beam assemblages accounting for warping constraints and rotation-dependency of moments." *Int. J. Numer. Methods Engrg.*, 33, 469-502. ,1992
13. Yang, Y. B. and McGuire, W., "Joint rotations and geometric nonlinear analysis. " *J. Struct. Eng. ASCE,* 112, 879-905.,1986